Quantum chaos, delocalization, and entanglement in disordered Heisenberg models

Winton G. Brown,[1,*] Lea F. Santos,[1,†] David J. Starling,[2] and Lorenza Viola[1,‡]
[1]*Department of Physics and Astronomy, Dartmouth College, 6127 Wilder Laboratory, Hanover, New Hampshire 03755, USA*
[2]*Department of Physics and Astronomy, University of Rochester, Rochester, NY 14627, USA*
(Received 6 July 2007; published 7 February 2008)

We investigate disordered one- and two-dimensional Heisenberg spin lattices across the transition from integrability to quantum chaos from both statistical many-body and quantum-information perspectives. Special emphasis is devoted to quantitatively exploring the interplay between eigenvector statistics, delocalization, and entanglement in the presence of nontrivial symmetries. The implication of the basis dependence of state delocalization indicators (such as the number of principal components) is addressed, and a measure of relative delocalization is proposed in order to robustly characterize the onset of chaos in the presence of disorder. Both standard multipartite and generalized entanglement are investigated in a wide parameter regime by using a family of spin- and fermion-purity measures, their dependence on delocalization and on energy spectrum statistics being examined. A distinctive correlation between entanglement, delocalization, and integrability is uncovered, which may be generic to systems described by the two-body random ensemble and may point to a new diagnostic tool for quantum chaos. Analytical estimates for typical entanglement of random pure states restricted to a proper subspace of the full Hilbert space are also established and compared with random matrix theory predictions.

DOI: 10.1103/PhysRevE.77.021106 PACS number(s): 05.30.−d, 05.45.Mt, 03.67.Mn, 03.67.Lx

I. INTRODUCTION

The emergence of nonintegrable behavior in quantum mechanics is a fascinating and widespread phenomenon which is largely responsible for the "complexity" intrinsic to the physical and mathematical description of interacting many-body quantum systems. A most striking consequence is the existence of distinctive quantum-chaotic properties for dynamical systems which may lack a clear classical limit. The characterization of such quantum chaos signatures has a long history, pioneered by Wigner in his effort to quantitatively model complex nuclei [1], and eventually culminating in statistical approaches to complex quantum systems based on so-called random matrix theory (RMT) [2–4].

Recent years have witnessed a renewed interest in qualitatively reassessing and quantitatively exploring many-body quantum complexity and quantum chaos implications in the light of quantum-information science (QIS) [5,6]. On one hand, a deeper understanding of quantum chaos and its implications is a prerequisite for identifying potentially harmful consequences as well as beneficial uses of chaos in information-processing devices: While the possibility that disorder may destabilize quantum computation through a "chaotic melting" [7,8] calls for careful hardware design and error control, chaotic evolutions tend to naturally generate effectively *random* states which are a resource for a variety of QIS protocols [9]. On the other hand, QIS provides additional tools for describing complexity of states and evolutions, which are proving useful in a variety of settings at the interface with condensed-matter and statistical physics. The notion of *entanglement*, in particular—as capturing distinctively quantum correlations which admit no local classical interpretation [10]—plays a central role to this end. Among the most notable developments to date, entanglement theory has allowed a considerably deeper understanding of quantum critical phenomena—appropriate entanglement measures serving as an "order parameter" for detecting and classifying quantum phase transitions in matter [11]—and to devise enhanced computational methods for both static and time-dependent properties of quantum lattice systems [12].

In this context, uncovering the relationship between various aspects of complexity in quantum states and evolutions, quantum chaos, and entanglement is both a natural and fundamental challenge, which is spurring significant activity in the field; see, e.g., [13–23] for representative contributions. In particular, specific questions to be answered include the following: What entanglement properties best capture the *structural change* occurring in typical many-body eigenstates across a transition to quantum chaos, and how well do such properties reflect the complexity of chaotic eigenstates? To what extent does the amount of entanglement relate to the amount of underlying *state delocalization*? Perhaps most importantly, can entanglement theory suggest *new signatures* of quantum chaos?

Our goal in this work is to take a step toward answering some of the above questions, by seeking an in-depth characterization of entanglement properties of the stationary states (eigenvectors) of nonintegrable as opposed to integrable many-body Hamiltonians, in relation to the behavior of traditional complexity indicators related to RMT spectral statistics and delocalization measures. In this respect, our analysis shares some motivation with earlier studies of entanglement across a transition to nonintegrability in a class of one-dimensional Harper Hamiltonians by Lakshminarayan *et al.* [24], and spin-1/2 lattice systems by Santos *et al.* [25] and Mejia-Monasterio *et al.* [26], where, however, primary emphasis is given to *pairwise* and *bipartite* entanglement. Only

*Winton.G.Brown@Dartmouth.edu
†Present address: Department of Physics, Yeshiva University, New York, NY 10016, USA. lsantos2@yu.edu
‡Corresponding author. Lorenza.Viola@Dartmouth.edu

recently has genuine *multipartite* entanglement started to be addressed, notably in the one-dimensional Ising model with a tilted magnetic field [21,27].

Here, we focus on a representative class of *disordered Heisenberg models*, which have received limited attention to date in spite of their prominent role in condensed-matter physics as well as in exchange-based circuit-model [28–34] and cluster-state [35] quantum computing architectures. As a further distinctive feature of our work, the notion of *generalized entanglement* (GE), introduced by Barnum *et al.* in [36,37], is exploited to both obtain a unified approach to standard (qubit-based) multipartite entanglement—quantified by a family of coarse-grained (spin-)purity measures—and to construct GE measures directly probing correlations in different (fermionic) operator languages. From this point of view, the present study further validates the usefulness of GE for broadly characterizing complexity in quantum systems, as recently demonstrated in applications to ground-state quantum phase transitions [38], chaotic quantum maps [39], and efficient solvability of Lie-algebraic models [40].

The content of the paper is organized as follows. We begin in Sec. II by recalling the essential RMT background, along with well-established spectral signatures of quantum chaos and measures of pure-state delocalization. Section III introduces the relevant class of one- (1D) and two-dimensional (2D) Heisenberg models, laying out the static disorder settings under examination (associated with randomness in the one-body energies, the two-body interactions, or both), and discussing the symmetries associated with different parameter regimes. A thorough characterization of integrability properties is obtained in Sec. IV, with the twofold objective of distinguishing between delocalized-localized regions and chaotic-integrable ones. The implications of the dependence of delocalization upon the basis choice are elucidated, and a measure of relative delocalization is introduced to gain additional insight into the properties of eigenvectors in disorder-induced chaotic regimes. After a brief account of entanglement and GE measures in Sec. V, we present in Sec. VI a detailed analysis of entanglement as a function of disorder strength and energy, as well as delocalization properties. As a main emerging feature, a strong and persistent correlation between multipartite entanglement and delocalization is found in nonintegrable regimes, which is consistent with independent evidence in [27] and may suggest a novel signature of quantum chaos. While most results are numerical, analytical estimates for multipartite entanglement of random pure states localized to a subspace are obtained in order to compare numerical results with RMT predictions. Throughout the paper, special care is devoted to contrast properties which are general to disordered spin-1/2 lattices to those which are specific to the Heisenberg interaction. The paper concludes with a summary and outlook in Sec. VII, followed by an appendix which collects technical derivations.

II. SIGNATURES OF QUANTUM CHAOS

It is well established that quantized versions of classically integrable and fully chaotic systems can be distinguished by their quantum energy level statistics [1,3,4,41–43]. Of particular interest is the distribution of energy level spacings, $P(s)$, where s is the spacing between neighboring energy levels after the spectrum has been appropriately unfolded, so that the density of states is everywhere equal to 1. Integrable systems typically exhibit a Poisson distribution,

$$P_{\mathrm{P}}(s) = \exp(-s), \quad s \in \mathbb{R}^+, \tag{1}$$

whereas chaotic systems have an energy level spacing distribution predicted by RMT. Within RMT, an exact description of a complex physical system is replaced by a statistical description based on ensembles of random matrices which share the same fundamental symmetry properties as the original system Hamiltonian. In particular, for the wide class of systems exhibiting time reversal invariance, the appropriate ensemble is the so-called Gaussian orthogonal ensemble (GOE), whose energy level spacing distribution is closely approximated by the Wigner-Dyson distribution,

$$P_{\mathrm{WD}}(s) = \frac{\pi s}{2}\exp\left(-\frac{\pi s^2}{4}\right), \quad s \in \mathbb{R}^+. \tag{2}$$

The eigenvectors of fully chaotic systems may also be described statistically using RMT. If the system of interest obeys time-reversal symmetry, the eigenvector components tend to follow a Gaussian distribution, resulting from the invariance of the GOE under arbitrary orthogonal transformations [41].

It is important to appreciate that systems such as interacting lattices of spin-1/2 particles have no obvious classical limit; thus the question of whether or not they may exhibit chaos must be posed and answered from an entirely quantum-mechanical perspective. Because the standard defining features of classical chaos (phase-space ergodicity and exponential divergence of neighboring trajectories) have no direct meaning for Hamiltonian quantum dynamical systems, neither does an unambiguously established framework exist for consistently defining integrability in quantum settings [44,45]; this issue is not straightforward and is still largely open. In the present context, we shall use the term "quantum chaos" in an operational sense, to simply mean the presence of RMT energy level statistics.

In order to examine the transition from integrability to chaos, the following picture is employed [26,41,46]. Let H_0 be an integrable Hamiltonian, that is, one for which the eigenvalues and eigenvectors may be determined analytically [40,47]. Now consider the effect of an integrability-breaking perturbation H', so that the total Hamiltonian becomes

$$H = H_0 + \lambda H', \quad \lambda \in \mathbb{R}^+. \tag{3}$$

For sufficiently small values of the parameter λ, the eigenvalues and eigenvectors of H are adequately described by perturbation theory. As λ increases to the point where the interaction strength between states that are directly coupled by H' is equal to their unperturbed energy difference [7,8], perturbation theory breaks down, and a crossover from a Poisson to a Wigner-Dyson distribution occurs. In parallel with such a crossover in energy level statistics, the eigenvectors of H become increasingly delocalized across the eigen-

states of H_0. As λ increases further, delocalization typically continues until the component distribution of the eigenvectors becomes that of GOE random states. The exact relationship between the level statistics and delocalization border has been much studied and remains in general an open question [7,8,48].

In order to identify parameter ranges where chaos is present, it is necessary to quantify how accurately the statistical properties of the eigenvalues and eigenvectors of the Hamiltonian are described by RMT. Here, we will address this question by examining the energy level and eigenvector statistics across the full spectrum, rather than restricting ourselves to a specific spectral region (see also Sec. IV C for additional quantitative discussion of this point).

The extent to which the energy level spacing distribution interpolates between the Poisson and Wigner-Dyson limits may be conveniently parametrized by a so-called level statistics indicator (LSI), introduced in [49]:

$$\eta \equiv \frac{\int_0^{s_o} [P(s) - P_{\mathrm{WD}}(s)]ds}{\int_0^{s_o} [P_{\mathrm{P}}(s) - P_{\mathrm{WD}}(s)]ds}, \tag{4}$$

where $s_0 \approx 0.4729$ is the first intersection point of $P_{\mathrm{P}}(s)$ and $P_{\mathrm{WD}}(s)$. The LSI has the value $\eta=1$ when $P(s)=P_{\mathrm{P}}(s)$, but $\eta=0$ if $P(s)=P_{\mathrm{WD}}(s)$.

In order to characterize the degree of eigenvector delocalization, a convenient measure is the so-called number of principal components (NPC) [2,50,51]. Given a basis $\{|n\rangle\}$ of the system Hilbert space $\mathcal{H}$, the NPC of a normalized pure-state vector $|\psi\rangle$ is defined as follows:

$$\xi(|\psi\rangle) \equiv \left(\sum_n |\langle n|\psi\rangle|^4\right)^{-1}. \tag{5}$$

Thus, the NPC estimates the number of basis states relative to which $|\psi\rangle$ has a significant component. For example, if $|\psi\rangle$ is a uniform superposition of exactly m basis states, then $\xi(|\psi\rangle)=m$. For an N-dimensional state vector with a component distribution pertaining to the GOE, the expected NPC is given by

$$\xi_{\mathrm{GOE}} = \frac{N+2}{3},$$

where the factor 1/3 emerges from the Gaussian fluctuations of the eigenstates, and the additive correction 2 is due to normalization [4,52]. Since N is usually large, the approximation $\xi_{\mathrm{GOE}} \sim N/3$ is commonly adopted. In parallel with the fact that the LSI as constructed takes into account the level statistics across the full spectrum, we will be primarily interested in the average value of the NPC across all of the eigenvectors in a relevant subspace.

III. DISORDERED HEISENBERG MODELS

The Heisenberg model in one and two spatial dimensions plays a paradigmatic role in condensed-matter physics and statistical mechanics as a testbed for exploring quantum magnetism and spin dynamics in reduced dimensionality [53]. Thus, an accurate characterization of its integrability properties in physical regimes of interest has both a fundamental and practical significance. In the special case of spin-1/2 particles, a partial characterization of the integrability-to-chaos transition has been achieved, based on both *clean* systems where chaos is induced by coupling two different spin chains [54] or by adding next-nearest-neighbor interactions [54–56], and on *disordered* systems, where the integrability-breaking term consists of random magnetic fields applied to all or a subset of spins [57–59]. Aside from their relevance to model real materials, disordered systems offer the added advantage of providing a natural arena to study the interplay between interaction and disorder, which remains a most challenging problem in condensed-matter physics.

Within QIS, the isotropic Heisenberg spin-1/2 model in an external magnetic field arises naturally in some of the most promising solid-state proposals for scalable quantum computation, each spin corresponding, in the simplest settings, to a logical qubit, and the exchange interaction providing the required interqubit coupling. Following the original suggestion by Loss and DiVincenzo [28] for coupling electron-spin qubits via tunable Heisenberg interactions in semiconductor quantum dots, schemes for effecting exchange-based universal quantum computation have been further developed for both electron [60] and donor-atom nuclear spins [30], constructive methods for universal quantum gate design and efficient readout being identified in [61]. In addition, scalable universal architectures where always-on Heisenberg couplings are used in conjunction with appropriate encodings of a logical qubit into three or more physical spins have been constructed, offering both substantial implementation flexibility [29] and enhanced decoherence suppression [32,62].

Depending on implementation details, imperfect qubit fabrication and/or uncontrolled residual spin-spin couplings during storage or gating may introduce an integrability-breaking perturbation H', causing the prerequisite mapping to well-defined logical qubits to be lost. While a number of error control schemes exist in principle to counteract the effects of H' (notably, dynamical refocusing methods for static disorder as considered here; see, e.g., [63]), understanding the error behavior due to H' remains an important preliminary step.

The Hamiltonian for an L-site lattice of spin-1/2 particles coupled by the Heisenberg interaction and subject to a bias field in the z direction is given by

$$H = \sum_{i=1}^{L} \frac{\varepsilon_i}{2}\sigma_z^{(i)} + \sum_{\{i,j\}} \frac{J_{ij}}{4}\vec{\sigma}^{(i)} \cdot \vec{\sigma}^{(j)}, \tag{6}$$

where $\vec{\sigma}^{(i)}$ is the vector of Pauli matrices $(\sigma_x^{(i)}, \sigma_y^{(i)}, \sigma_z^{(i)})$ acting on the two-dimensional Hilbert space of the ith site. The parameter ε_i determines the on-site Zeeman energy of the ith spin, and will be parametrized as $\varepsilon_i = \varepsilon + \delta\varepsilon_i$, where ε is a nonzero average and $\delta\varepsilon_i$ are uniformly distributed within $[-\delta\varepsilon/2, \delta\varepsilon/2]$, characterizing the different strengths of local random magnetic fields. The interaction strength between spins i and j is given by J_{ij}, which will be likewise param-

etrized as $J_{ij}=J+\delta J_{ij}$, where J is the average coupling and δJ_{ij} represents random interactions, being uniformly distributed in $[-\delta J/2, \delta J/2]$ [64]. Since we are interested in the whole spectrum, the sign of the exchange coupling parameter J is irrelevant. In the numerical simulations, we shall assume $J \geq 0$. The set of interacting pairs $\{i,j\}$ is determined by the topology of the lattice. We shall consider nearest-neighbor interactions on a 1D chain and on a 2D rectangular lattice. In addition, the following notation is introduced:

$$H_Z = \sum_{i=1}^{L} \frac{\varepsilon_i}{2} \sigma_z^{(i)}, \tag{7}$$

$$H_J = \frac{J}{4} \sum_{i=1}^{L-1} \vec{\sigma}^{(i)} \cdot \vec{\sigma}^{(i+1)}. \tag{8}$$

As discussed in Sec. IV, these two terms correspond to integrable limits of the Hamiltonian given in Eq. (6).

A. Two-body random ensemble

It is important to appreciate that the class of systems considered here [Eq. (6)] is more accurately described by the *two-body random ensemble* (TBRE), which, instead of L-body couplings as implicit in the GOE, involves only two-body interactions. The TBRE, and more broadly the embedded Gaussian ensembles with k-body interactions ($k<L$), was introduced in [65,66] as a physically more realistic statistical setting for describing few-body interacting systems, such as atoms, molecules, and nuclei. Among the differences between the two ensembles [67–69], we highlight the ones that are most directly relevant to this work.

(1) The GOE local density of states (also called the LDOS profile; see, e.g., [7,50]) as a function of energy shows a semicircular law, whereas it is Gaussian for the TBRE.

(2) The TBRE lacks ergodicity, in the sense that the statistical properties of each ensemble member need not coincide with the ensemble average [70].

(3) In contrast to the energy-independent NPC value predicted by the GOE, the NPC estimate for the TBRE shows a strong variation with the energy of the state, approaching the GOE prediction of $N/3$ mostly in the middle of the energy spectrum.

B. Relevant symmetries

Although integrability may be regarded as equivalent to the presence of a complete set of symmetries of the defining Hamiltonian [71], if such a set is incomplete then chaos may still be present within distinct symmetry sectors. However, a Wigner-Dyson distribution occurring independently in different sectors will tend to be washed out if the corresponding energy levels are mixed together. Thus, in order for clear conclusions to be drawn based on the energy level statistics, it is necessary to desymmetrize the spectrum according to its trivial symmetries, that is, the level spacing distribution must be examined separately in each resulting symmetry sector. The symmetries of the Hamiltonian in Eq. (6) are determined by the choice of model parameters ε_i and J_{ij}:

(1) *Rotational symmetry around the z axis*. For all values of ε_i and J_{ij}, the z component of the total spin, $S_z=\Sigma_i \sigma_z^{(i)}/2$, is a conserved quantum number, that is, $[S_z,H]=0$. For even L, the largest subspace corresponds to $S_z=0$, having dimension $N_0=\binom{L}{L/2}=L!/[(L/2)!]^2$. We shall focus primarily on this subspace, $\mathcal{H}_0$, as chaos sets in here first. A natural basis for $\mathcal{H}_0$ is the one associated with the eigenstates of H_Z, which will be referred to as the *computational basis* or simply c basis.

(2) *Conservation of total spin.* When the on-site energies are degenerate, $\varepsilon_i=\varepsilon$, the total spin $S^2=(\Sigma_i \vec{\sigma}^{(i)}/2)^2$ also becomes a good quantum number, $[S^2,H]=0$. Therefore, in this parameter regime the system must be separately studied in each symmetry sector characterized by fixed quantum numbers S_z and S [72].

(3) *Symmetries due to lattice geometry.* For $\varepsilon_i=\varepsilon$ and $J_{ij}=J$, symmetries under site permutations related to the geometry of the lattice must also be considered. Under periodic boundary conditions, H is invariant under cyclic translations and reflections of the lattice sites, resulting in momentum and parity conservation, respectively. Note that, in rectangular 2D lattices, momentum and parity in both directions are good quantum numbers. For open boundary conditions, the Hamiltonian is invariant under lattice reflections only. We shall restrict our analysis to *open boundary conditions* in what follows, because they lead to fewer symmetries and hence larger invariant subspaces, which permit better eigenvalue statistics. Therefore, when identifying invariant subspaces, the eigenstates will be grouped according to their quantum numbers (S_z,S,R), where R indicates parity.

(4) *Time-reversal invariance.* The GOE is the ensemble appropriate for describing the static properties of systems exhibiting time-reversal invariance, that is, for Hamiltonians that commute with the time-reversal operator $T_0=(i)^L \otimes_{j=1}^{L} \sigma_y^{(j)} K$, where K is the conjugation operator in the c basis for spin 1/2. It is important to note that the Heisenberg model with a magnetic field does not commute with the conventional time-reversal operator T_0. Nevertheless, the GOE rather than the more general Gaussian unitary ensemble is appropriate for this model because the Hamiltonian matrix admits a straightforward *real* representation in the c basis. Equivalently, one may understand the applicability of the GOE as resulting from the fact that the Hamiltonian is invariant under K which may be regarded as a nonstandard time-reversal operator as in [41,57].

Although, as mentioned, for a fully established (or weakly broken) symmetry one may examine the level statistics in each invariant subspace, for strongly broken symmetry it is no longer possible to sort eigenvalues by symmetry quantum numbers, nor can correlations between different subspaces be ignored. As a result, separating the effect of symmetries on the energy level spacing distribution from that of integrability vs chaos becomes challenging throughout the symmetry transition regime, that is, it is difficult to distinguish systematically between the emergence of a complete vs incomplete set of symmetries. While some analytical results exist for eigenvalue statistics across the full space in the presence of symmetry breaking [73,74], they do not offer a practical diagnostic tool for distinguishing between fully chaotic and

partly integrable behavior in broken-symmetry regimes based on the LSI (especially when multiple symmetry subspaces are involved as in the S^2-symmetry breaking which plays a relevant role here).

C. Related models

The Heisenberg model may be regarded as one of a related class of spin-1/2 lattice models with two-body interaction Hamiltonians of the form

$$H_{XYZ} = \sum_i \varepsilon_i \sigma_z^i + \sum_{\{i,j\}} (J_{ij}^x \sigma_x^{(i)} \sigma_x^{(j)} + J_{ij}^y \sigma_y^{(i)} \sigma_y^{(j)} + J_{ij}^z \sigma_z^{(i)} \sigma_z^{(j)}).$$

In particular, the 2D Ising model in a transverse field ($J_{ij}^z = J_{ij}^y = 0$), as well as the XXZ model ($J_{ij}^x = J_{ij}^y, J_{ij}^z \neq 0$) and the isotropic XY model ($J_{ij}^x = J_{ij}^y, J_{ij}^z = 0$), have been previously studied in the context of quantum computation and quantum chaos [7,8,25,26,75,76]. However, the Heisenberg model differs in some essential characteristics, notably the nontrivial role of symmetries. Also distinctive in the Heisenberg exchange coupling is the competing nature of the two interacting terms in the Hamiltonian: in the c basis, the diagonal Ising interaction $\sigma_z^{(i)} \sigma_z^{(j)}$ favors localization, whereas the flip-flop term $\sigma_x^{(i)} \sigma_x^{(j)} + \sigma_y^{(i)} \sigma_y^{(j)}$ induces delocalization. Thus, a comparison between our results and those of previous studies will also serve to identify those properties that are generic to disordered spin-1/2 lattices as contrasted to those specific to the Heisenberg model.

IV. RESULTS: LEVEL STATISTICS AND DELOCALIZATION PROPERTIES

We shall proceed by first obtaining a basic characterization of the level spacing distribution and average delocalization properties of the eigenvectors for a wide range of parameters of interest, and then proceed to examining entanglement properties in Sec. VI.

A. From integrability to chaos

The model described by Eq. (6) shows two limiting integrable cases H_Z and H_J [Eqs. (7) and (8), respectively]. The first is a trivially solvable noninteracting problem, while the second is solvable only in 1D by the Bethe ansatz [77–80]. A transition to chaos may be induced by adding an integrability-breaking term to any of the two integrable limits. Here, we shall focus on the following representative scenarios.

Case $J/\delta\varepsilon$. Exchange interactions with a constant strength J are added to $H_0 = H_Z$. The crossover between integrability and chaos is studied as a function of the ratio $J/\delta\varepsilon$, with $\delta J = 0$ throughout.

Case $\delta J/J$. Exchange interactions with random strength are added to $H_0 = H_J$. The crossover between integrability and chaos is analyzed as a function of the ratio $\delta J/J$, with $\delta\varepsilon = 0$ throughout.

Case $\delta J/\delta\varepsilon$. Exchange interactions with random strength are added to $H_0 = H_Z$. The crossover between integrability and chaos is studied as a function of the ration $\delta J/\delta\varepsilon$.

Clearly, case $J/\delta\varepsilon$ includes the other two cases in limiting situations: Specifically, it coincides with case $\delta J/\delta\varepsilon$ when the on-site disorder dominates over the disorder in the coupling strengths, $\delta\varepsilon \to \infty$, and with case $J/\delta\varepsilon$ when the distribution of coupling strengths is very narrow, $J \to \infty$.

B. Delocalization measures

Because the properties of a state vector (in particular, delocalization) depend entirely on the choice of representation, quantities such as the NPC cannot serve as intrinsic (basis-independent) indicators of quantum chaos, such as energy level statistics are considered to be. This fact may undermine the entire program of establishing connections between the properties of the eigenvectors of a Hamiltonian and its level of chaoticity. Yet it is well known that, for chaotic Hamiltonians, RMT predictions hold (to some extent) in a large number of reasonable representations, although a systematic characterization of such representations and the degree of agreement one may expect remain at present unanswered questions. Here, we conform to the standard approach to this problem, and examine eigenvector properties with respect to a basis in which the spread of the eigenvectors has a physical meaning, for instance one which relates to the relevant measurement capabilities, or to an integrable limit of the class of Hamiltonians under consideration. On one hand, we shall investigate to what extent the eigenvector properties associated with quantum chaos depend on the choice of two different bases corresponding to the integrable limits (7) and (8). On the other hand, we shall introduce a measure of relative delocalization between bases associated with different disorder realizations. Specifically, we will examine the following.

(i) The above-mentioned c basis, which is associated with the eigenstates of H_Z. In quantum computation, this is the basis that represents classical information, relative to which the final readout measurement is performed [5]. The associated NPC will be labeled ξ_c.

(ii) A so-called J basis, or interaction basis, which corresponds to the eigenbasis of H_J. In this case, the associated NPC will be denoted by ξ_J.

(iii) A disorder-dependent relative representation, which is obtained as follows. Within a set of sequentially generated random realizations, the eigenbasis of a given random realization is used to calculate the NPC for the eigenvectors of the subsequent realization. The associated NPC, which will be denoted ξ_r, quantifies relative delocalization, that is, how delocalized are the eigenbases associated with different disorder realizations with respect to each other, rather than with respect to some fixed basis. By construction, this quantity is independent of any fixed basis and depends only on the disorder.

Interestingly, an approach that attempts to quantify the complexity of the eigenstates of an ensemble of Hamiltonians in a way similar to the above-mentioned relative delocalization has been proposed based on the notion of correlational entropy [81]. Both correlational entropy and relative delocalization overcome the problem of basis dependence by invoking a distribution over Hamiltonians. An important difference, however, is that evaluating the correlational entropy

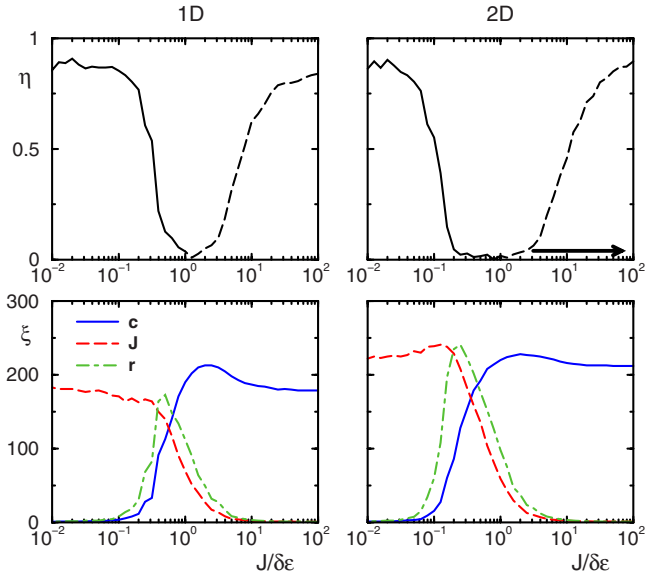

FIG. 1. (Color online) Case $J/\delta\varepsilon$, $S_z=0$ subspace, $L=12$. Top panels: Level statistics indicator η vs $J/\delta\varepsilon$. The dashed line indicates in each case the transition region, where the (S,R) subspaces are not fully distinct. The arrow indicates the actual limiting value of the LSI as $J/\delta\varepsilon\to\infty$. Bottom panels: Number of principal components ξ vs $J/\delta\varepsilon$. Left panels: 1D chain. Right panels: 2D 3×4 lattice. Averages over 20 random realizations.

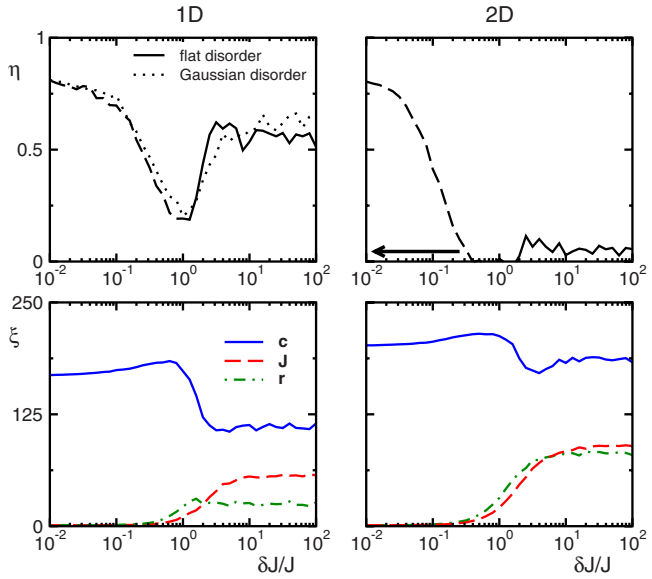

FIG. 2. (Color online) Case $\delta J/J$, $(S_z,S)=(0,1)$ subspace, $L=12$. Top panels: Level statistics indicator η vs $\delta J/J$. Dashed lines indicate in each case the region where the transition to R-symmetry sectors occurs. Dotted line: Gaussian disorder with $\sigma=\delta J/4$. The arrow indicates the actual limiting value of η as $\delta J/J\to0$. Bottom panels: Number of principal components ξ vs $\delta J/J$. Left panels: 1D chain. Right panels: 3×4 lattice. Averages over 50 random realizations.

requires tracking individual eigenstates as a function of the disorder across the full disorder space. While a further comparison between the two concepts would be worth pursuing, it is likely that this feature could make relative delocalization computationally more tractable for many disorder settings.

C. Numerical results

We consider the $S_z=0$ subspace $\mathcal{H}_0$ for 1D and 2D models. In both cases, for lattice size $L=12$, $\dim(\mathcal{H}_0)=N_0=924$. As anticipated in Sec. II, NPC values are averaged over all eigenstates in $\mathcal{H}_0$, and both the LSI and NPC are further averaged over a number of disorder realizations sufficient for accurate statistics, as indicated in each figure caption.

Case $J/\delta\varepsilon$. For this disorder setting, two integrability-chaos transitions are verified for the 1D model, whereas only one occurs in 2D. From the top panels of Fig. 1, we see that in both cases the first crossover, from the H_Z integrable limit to chaos, is observed as the interaction strength J increases from zero to a value close to the energy difference between directly coupled states, $J/\delta\varepsilon\sim1$. In the other extreme, where $J/\delta\varepsilon\to\infty$ and therefore $H\to H_J$, the transition to S^2 and R symmetry complicates the interpretation of the energy level statistics. During this transition, different (S,R) invariant subspaces partially overlap, and the observed LSI increase across the whole $S_z=0$ subspace need not reflect a change toward integrability, but rather the progressive decoupling of states belonging to different subspaces (this region is indicated by a dashed line in the figure). Once the transition is complete, at $J/\delta\varepsilon\to\infty$, the level spacing distribution within individual (S_z,S,R) symmetry sectors may be determined. This results in a Poisson distribution for the 1D model [82], consistent with its exact solvability. However, and contrary to the behavior of the LSI across the whole $\mathcal{H}_0$, the level spacing distribution in the invariant subspaces of the 2D system is strongly Wigner-Dyson.

It is interesting to contrast the LSI results with those for the NPC. The dependence of ξ_c, ξ_J, and ξ_r on $J/\delta\varepsilon$ is illustrated in the bottom panels of Fig. 1. Corresponding to the broader chaotic region detected by the LSI, there is greater delocalization in 2D, especially as quantified by ξ_J and ξ_r. For both cases, the maximum NPC in most instances occurs within the chaotic region, which we take to be $\eta\lesssim0.3$ [7]. However, the actual value falls short of the RMT prediction and different NPC measures may disagree substantially even within the chaotic region. For example, at $J/\delta\varepsilon\approx2$ where ξ_c reaches its maximum, ξ_J and ξ_r show only partial delocalization. ξ_c and ξ_J detect only one localized-to-delocalized transition, whereas ξ_r is only large where the LSI is low. Note that the behavior of ξ_r matches more closely the behavior of the LSI on the transition in LSI occurring at low values of $J/\delta\varepsilon$ than ξ_c. However, in the limit $J/\delta\varepsilon\to\infty$, ξ_r fails to discriminate between the integrability of the 1D model and the presence of chaos in the 2D model, decreasing to 1 in both cases due to the absence of disorder.

Case $\delta J/J$. In this case, $[S^2,H]=0$, thus we examine the LSI and NPC in the largest S^2 subspace, corresponding to $S=1$ and dimension $N=297$ eigenstates. As $\delta J/J\to0$ ($H\to H_J$), the reflection symmetry becomes important, causing the LSI in the top panels of Fig. 2 to increase irrespective of the chaoticity or integrability of the Hamiltonian. As previously discussed, in this limit the 1D model is integrable,

while the 2D model is not. Consequently, as $\delta J/J$ increases from 0, a transition from integrability to chaos occurs for the 1D model, whereas only the breaking of the reflection symmetries occurs in the 2D model. Notably, for the 1D model near $\delta J/J=2$, an unexpected rapid transition in the LSI from $\eta\sim 0.2$ to an intermediate value of $\eta\sim 0.6$ is observed. Although the 2D system remains chaotic throughout, a small rise in LSI close to $\delta J/J\sim 2$ is noticeable.

The NPC values are shown in the bottom panels of Fig. 2. Since the Hamiltonians in the J basis and in any basis associated with a disorder realization are block diagonal, ξ_J and ξ_r cannot exceed the dimension of the $(S_z,S)=(0,1)$ subspace, unlike ξ_c, which is upper-bounded only by the dimension of the $S_z=0$ subspace, given that states of the c basis do not posses S^2 symmetry. For the 1D model, the slight increase in ξ_c as $\delta J/J\to 1$ occurs during the integrability-chaos transition, but the same occurs also for the 2D system, which is chaotic throughout. Thus, this increase is likely related to the reflection-symmetry breaking. Interestingly, the abrupt drop in ξ_c for both 1D and 2D near $\delta J/J=2$ appears to be connected with the rise in the LSI—the greater change in both LSI and ξ_c occurring for the 1D model.

A possible explanation for the observed transition at $\delta J/J\sim 2$ is based on the fact that this value marks the point where interaction strengths arbitrarily close to zero are allowed, $\min_{ij}\{J_{ij}\}=J-\delta J/2=0$. If the chain is broken into two or more approximately uncoupled segments, then the energy spectrum of each segment becomes approximately independent. Even if for each segment the level spacing distribution is Wigner-Dyson, the level spacing distribution for the combined spectrum will not be. Lending support to this explanation is the far stronger effect in 1D than in 2D, following from the fact that the 2D lattice cannot be as easily broken into isolated segments. In order to determine if this effect is an artifact of the sharp cutoff in the disorder distribution, interactions with Gaussian disorder (with standard deviation $\sigma=\delta J/4$) were also examined. The results are shown as the dotted line in Fig. 2 (top left), where it is seen that the abrupt transition remains despite the absence of a sharp cutoff in the disorder range (note, however, that the width of the transition is affected).

It is intriguing to notice that in 1D the ground-state and low-energy excitations for this disorder setting have been determined at $\delta J/J=2$ through an exact renormalization group approach, and are known to be described by the *random singlet phase* [83–85]. A more thorough discussion of possible connections between the observed behavior and the existence of a random singlet phase are left for future investigation.

As a further remark, the behavior of ξ_r in the region where $\delta J/J>2$ is worth mentioning. In 1D, ξ_r is much lower than ξ_J, while in 2D only a small difference is seen. This further demonstrates that, in the presence of disorder, relative delocalization can be an effective indicator of chaos.

Case $\delta J/\delta\varepsilon$. The dependence of the LSI on $\delta J/\delta\varepsilon$ is shown in the top panels of Fig. 3. As the disorder in the coupling strengths becomes sufficiently large to compete with the energy difference $\delta\varepsilon$, a transition from integrability to fully developed chaos is observed only for the 2D model, whereas in 1D the LSI merely approaches an intermediate

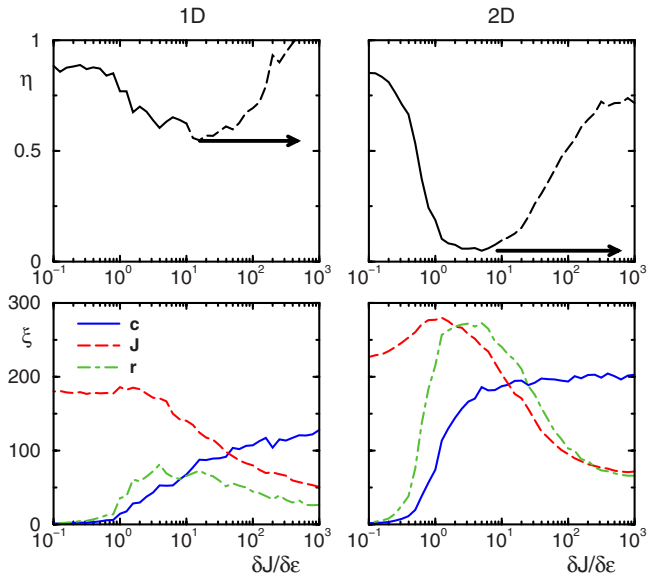

FIG. 3. (Color online) Case $\delta J/\delta\varepsilon$. $S_z=0$ subspace, $L=12$. Top panels: Level statistics indicator η vs $\delta J/\delta\varepsilon$. Dashed line indicates the region where the transition to S^2-symmetry sectors occurs. Arrow indicates the actual limiting value of η as $\delta J/\delta\varepsilon\to\infty$. Bottom panels: Number of principal components ξ vs $\delta J/\delta\varepsilon$. Left panels: 1D chain. Right panels: 3×4 lattice. Averages over 50 random realizations.

value of $\eta\sim 0.6$ [86]. For $\delta J/\delta\varepsilon\gtrsim 10$, the LSI for the entire $S_z=0$ subspace increases, but, as before, this does not necessarily reflect an approach to integrability, since a transition to the S^2 symmetry is in place. In fact, at $\delta J/\delta\varepsilon\to\infty$, we have verified that essentially the same LSI values reached at $\delta J/\delta\varepsilon\sim 10$ for 1D and 2D within the $(S_z,S)=(0,1)$ subspace are attained.

The NPC behavior is depicted in the bottom panels of Fig. 3. Reflecting the fact that chaos never fully develops in 1D, both ξ_c and ξ_r are considerably lower when compared to the previous case. In contrast, for the 2D model, this disorder setting leads to a high level of delocalization, especially in the J basis and in terms of relative delocalization. The maximum values are reached between $1\lesssim\delta J/\delta\varepsilon\lesssim 6$. As $\delta J/\delta\varepsilon$ increases further, the transition to S^2-symmetry sectors becomes relevant, and the Hamiltonians in these two representations approach a block-diagonal form—therefore ξ_J and ξ_r decrease accordingly. As $\delta J/\delta\varepsilon\to\infty$, the values obtained still indicate strong delocalization relative to the sizes of the $(0,S)$ subspaces.

Consistent with studies of the TBRE and of other systems with two-body interactions (notably, nuclear-shell models), a strong dependence of NPC on energy is observed, particulary in chaotic regions (see Fig. 4). Specifically, the NPC follows an approximately Gaussian form. We show a representative 2D case at $\delta J/\delta\varepsilon\sim 3$, where ξ_J and ξ_r are close to their maximum. Note that RMT provides a bound on the extent of delocalization, and that, even in the center of the spectrum, the average delocalization falls short of the predictions of RMT, particularly in the c basis. That the eigenstates in the tails of the spectrum are less delocalized than those in the center, however, only partially affects the average NPCs

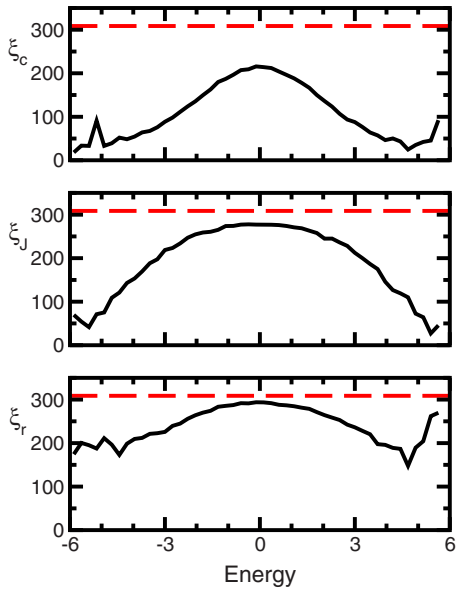

FIG. 4. (Color online) Case $\delta J/\delta\varepsilon$. Number of principal components vs energy eigenvalue for $\delta J/\delta\varepsilon=3$. Eigenstates in the $S_z=0$ subspace for a 3×4 qubit lattice are considered. The dashed horizontal line shows the GOE prediction $\xi_{\mathrm{GOE}}=(N_0+2)/3\sim308$. Averages over 20 random realizations.

shown in Figs. 1–3, because the density of states is also peaked around the center of the spectrum. We found that averaging only over the central 100 eigenstates (10.6% of the total) increases the values of each NPC measure by an amount between 10% and 15%, and does not qualitatively affect the behavior of the average NPC. For all cases except for ξ_J and ξ_r in the case $\delta J/\delta\varepsilon$ near their maxima, the deviation from the RMT prediction of $N/3$ remains substantial.

This situation is to be compared with the models studied in [7] and [26]. Even though these models also correspond to the TBRE, better agreement with RMT is obtained for delocalization whenever the interactions are either purely off diagonal or all-to-all, that is, every site is coupled with every other site. In fact, a key difference in our case is the presence of the purely diagonal Ising contribution, which favors localization in the computational basis. Furthermore, we have verified that all-to-all Heisenberg couplings also yield delocalization values in better agreement with RMT (data not shown). Thus, the lower level of ergodicity in the models examined here may be partly attributed to lower connectivity.

V. ENTANGLEMENT MEASURES

Obtaining a complete characterization of entanglement in many-body systems is a challenging problem which in spite of extensive effort remains as yet largely unsolved [11]. As a main reason for such difficulty, it is evident that no single entanglement measure can fully capture the complexity of multiparticle correlations. For our current purposes, we shall select representative measures of entanglement that both are computationally practical and directly connect with prior work on entanglement and quantum chaos and/or quantum phase transitions. Specifically, we shall investigate so-called concurrence between selected pairs of qubits as a measure of pairwise correlations [87], and a family of multipartite purity measures constructed within the general GE framework [36,37].

For a pure state $|\psi\rangle$ of two qubits, *concurrence* may be defined as

$$C(|\psi\rangle)=|\langle\psi|\sigma_y^{(1)}\otimes\sigma_y^{(2)}|\psi^*\rangle|,$$

where $|\psi^*\rangle$ is the complex conjugate of $|\psi\rangle$. Physically, $C(|\psi\rangle)$ may be thought of in this case as the overlap of a state with its time-reversed counterpart. When a pure state $|\psi\rangle$ of $L>2$ qubits is considered, the reduced two-qubit state of a selected pair (i,j) is described by a density matrix ρ_{ij}, where all but the qubits of interest are traced out. In this case, concurrence may be computed through a more general expression, which holds also for *mixed* states, and reads

$$C(\rho_{ij})=\max(0,\lambda_1-\lambda_2-\lambda_3-\lambda_4), \tag{9}$$

where $\lambda_1\geq\lambda_2\geq\lambda_3\geq\lambda_4$ are the square roots of the eigenvalues of $\rho_{ij}\tilde{\rho}_{ij}$, and $\tilde{\rho}_{ij}=(\sigma_y^{(1)}\otimes\sigma_y^{(2)})\,\rho_{ij}^*(\sigma_y^{(1)}\otimes\sigma_y^{(2)})$ [87]. Concurrence ranges from a minimum of 0 for unentangled states to a maximum of 1 for states containing a maximum amount of pairwise correlations. Thus, applied to a pair of qubits in a pure many-qubit state, zero concurrence will occur for a product state $|\psi\rangle=|\phi_1\rangle\otimes\cdots\otimes|\phi_L\rangle$, but also for the L-partite Greenberger-Horne-Zeilinger state $|\mathrm{GHZ}_L\rangle=\frac{1}{\sqrt{2}}(|0,\ldots,0\rangle+|1,\ldots,1\rangle)$, which exhibits genuinely multipartite correlations [88]. For random states of a sufficiently large number of qubits, the expected value of concurrence between any two qubits is very close to zero [89].

For a multipartite system, concurrence quantifies the amount of mixed-state bipartite entanglement within a given pair. Complementary information about how the pair itself, or, more generally, a given subset A of qubits, correlates with the remaining subset B, is provided by the amount of bipartite entanglement between A and B. The unique measure satisfying all requirements of invariance under local transformations, continuity, and additivity is the von Neumann entropy of either reduced density matrix, e.g.,

$$S(|\psi\rangle_{AB})=-\mathrm{Tr}_A(\rho_A\log_2\rho_A),$$

where ρ_A is the reduced density operator of subsystem A. If the additivity requirement is relaxed, a simpler linearized version of the above expression suffices to quantify bipartite entanglement, the so-called linear entropy,

$$E(|\psi\rangle_{AB})=1-\mathrm{Tr}_A(\rho_A)^2.$$

Although the amount of multipartite entanglement is generally hard to quantify away from bipartite states, useful indirect insight may be gained by considering different bipartitions of the system. In particular, $|\psi\rangle$ certainly contains genuine multipartite entanglement if no reduced subsystem state is pure.

The notion of GE offers a powerful framework for both organizing conventional multipartite entanglement within a unified setting, and for extending the concept of entangle-

ment to situations where a preferred partition of the system into subsystems may not be meaningful or otherwise desirable [36–38,90]. GE is based on the relationship of the state of interest to a distinguished set of observables, rather than to a tensor product decomposition of the Hilbert space $\mathcal{H}$ into subsystems. Let such a distinguished observable set consists of the Hermitian operators in a linear subspace h of the full operator space on $\mathcal{H}$, with h closed under Hermitian conjugation. The key step is to replace the notion of the subsystem state as obtained via the usual partial trace operation by the notion of a "reduced state" as determined by the expectation values of observables belonging to the restricted subspace h. A pure state $|\psi\rangle$ is generalized unentangled (entangled) relative to h depending on whether its reduced state is pure (mixed) in the space of all reduced states, that is, depending on whether it is *extremal* (or not) in the convex sense. If $\{B_i\}$ is a basis of Hermitian traceless operators for h, orthogonal in the trace inner product, a natural measure for GE is the degree of purity of the reduced h state as quantified by the *h-purity*,

$$P_h(|\psi\rangle) = \kappa \sum_i |\langle\psi|B_i|\psi\rangle|^2, \tag{10}$$

where the overall normalization constant κ is chosen so that P_h ranges between its maximum value of 1 for generalized unentangled states and its minimum value of 0 for maximal GE relative to h.

When the observable set h is the Lie algebra of all local observables on qubits, GE reduces to standard multipartite qubit entanglement. In particular, the above h-purity (10) relative to arbitrary single-qubit observables takes the explicit form

$$P_1(|\psi\rangle) = \frac{1}{L} \sum_{\alpha=x,y,z}^{i=1,L} |\langle\psi|\sigma_\alpha^{(i)}|\psi\rangle|^2. \tag{11}$$

This quantity is simply related to the so-called Meyer-Wallach measure of global entanglement, Q, by $P_1=1-Q$ [38,91,92], which quantifies multipartite entanglement through the average bipartite entanglement between one qubit and the rest. By construction, $P_1=1$ for product states, whereas $P_1=0$ for states such as $|\mathrm{GHZ}_L\rangle$, where each single-qubit reduced density matrix is totally mixed.

A family of related entanglement measures may be naturally constructed from the above local purity by coarse graining. If the qubits are partitioned into distinct n-qubit blocks, the *n –local purity*, denoted P_n, is defined as the purity with respect to arbitrary observables local to each block. For example, the bilocal purity (also used in [23]) is given by

$$P_2(|\psi\rangle) = \frac{2}{3L} \sum_{\alpha,\beta=x,y,z}^{i=1,L/2} |\langle\psi|\sigma_\alpha^{(2i-1)}\sigma_\beta^{(2i)}|\psi\rangle|^2, \tag{12}$$

where the sum only extends to traceless operators. Physically, the measure P_n, for $n>1$, ignores short-range correlations which P_1 detects. For the 1D chain we consider, the natural choice of partitions is into contiguous blocks. For the 2D lattice, relevant block partitions are illustrated in Fig. 5.

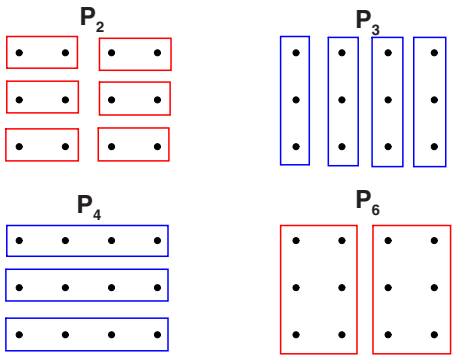

FIG. 5. (Color online) Choices of partitions for evaluating n–local purities in the 3×4 lattice.

It is important to mention that the von Neumann entropy of an n-qubit block, which has been a more broadly used quantity in studies of entanglement vs quantum chaos [19,20,26,27], is closely related in meaning to P_n. It can be shown that the average bipartite entanglement between the n-qubit block and the rest, $Q_n=1-P_n$, is (up to a normalization constant) equal to the average linear entropy over each n-qubit block participating in P_n. Thanks to the average over many blocks, P_n is less sensitive to edge effects. Apart from that, a main advantage with respect to von Neumann block entropy is its mathematical simplicity, which allows analytic calculations of the expected GE for random pure states and also reveals a quantitative relationship with delocalization as measured by the NPC in a local basis [93]. In particular, for random pure states with purely *real* components, as expected for GOE eigenvector statistics, the average value $\overline{P_n}$ with respect to the appropriate Haar measure may be exactly computed for arbitrary lattice size L. While we defer the details of the derivation to the Appendix, the results for states in the $S_z=0$ subspace with $L=12$ are summarized in Table I.

The intrinsic flexibility of the GE notion easily allows for the construction of purity measures relative to distinguished operator spaces not directly tied to a subsystem partition. For spin-1/2 systems, in particular, a natural choice of distinguished observables emerges upon mapping Pauli spin operators to canonical fermionic operators via the Jordan-Wigner transform,

$$c_j = (\otimes_{i=1}^{j-1}\sigma_z^{(i)})\sigma_+^{(j)}, \quad \sigma_+^{(j)} = \frac{1}{2}(\sigma_x^{(j)} + i\sigma_y^{(j)}).$$

It is straightforward to show that the $\{c_i\}$ satisfy canonical fermionic anticommutation relations $\{c_i^\dagger, c_j\}=\delta_{ij}$, $\{c_i, c_j\}=0$. Then "generalized local" resources may be associated with quadratic fermionic observables commuting with the total

TABLE I. Expected n–local purity for random states in the $S_z=0$ subspace of an $(L=12)$-site lattice, $N_0=924$. Values are multiplied by a factor of 10^3 for clarity.

$\overline{P_1}$	$\overline{P_2}$	$\overline{P_3}$	$\overline{P_4}$	$\overline{P_6}$
2.16	5.69	7.71	7.49	10.10

fermionic number operator, $\hat{L}=\Sigma_i c_i^\dagger c_i$—as opposed to "nonlocal" resources involved in processes where the total fermion number in a given pure state may change. The corresponding distinguished observable set is isomorphic to the unitary Lie algebra in L dimensions, $h=\mathfrak{u}(L)$. GE relative to such algebra is quantified by the fermionic $\mathfrak{u}(L)$-purity [38],

$$P_{\mathfrak{u}(L)}(|\psi\rangle)=\frac{2}{L}\sum_{i<j=1}^{L}(\langle c_i^\dagger c_j+c_j^\dagger c_i\rangle^2-\langle c_i^\dagger c_j-c_j^\dagger c_i\rangle^2)+\frac{4}{L}\sum_{i=1}^{L}\left\langle c_i^\dagger c_i-\frac{1}{2}\right\rangle^2. \quad (13)$$

Physically, $P_{\mathfrak{u}(L)}$ indicates how "close" a state is to being described by a fermionic product state (a Slater determinant) [90]. For example, in the two-excitation sector, $P_{\mathfrak{u}(L)}(|\psi\rangle)=1$ if and only if $|\psi\rangle$ may be written in the form $|\psi\rangle=c_a^\dagger c_b^\dagger|\mathrm{vac}\rangle$, where a,b label any set of modes unitarily related to modes i,j, and $|\mathrm{vac}\rangle$ contains no fermions. $P_{\mathfrak{u}(L)}$ has been shown to successfully detect and characterize broken-symmetry quantum phase transitions [38]. In the context of the transition to quantum chaos, such a measure may be expected to provide insight into entanglement generation associated with the departure from a noninteracting fermion problem.

VI. RESULTS: ENTANGLEMENT BEHAVIOR

We are now in a position to address entanglement properties of Heisenberg-model eigenvectors, and to understand the resulting behavior based on the insight gained from the corresponding behavior of delocalization and energy level statistics.

A. Disorder dependence

Case $J/\delta\varepsilon$. As remarked, this setting is especially useful for exploring possible connections between integrability-breaking, delocalization, and entanglement, because it contains both the integrable limits associated with H_Z (in 1D and 2D) and H_J (in 1D). With respect to the c basis, the 1D model possesses three regimes of interest: (i) integrability localization for $J/\delta\varepsilon\to 0$; (ii) chaos for intermediate ratios $J/\delta\varepsilon\sim 1$; and (iii) integrability delocalization for $J/\delta\varepsilon\to\infty$ in 1D, while in the last regime the 2D model remains strongly nonintegrable.

Figure 6 summarizes the behavior of the average concurrence between all neighboring spins, C, and of the n-local purities P_n for the 1D and 2D models. As we depart from the purely local Hamiltonian H_Z and $\delta J/\delta\varepsilon$ increases from 0 to 1, a peak in C is observed *before* the onset of chaos. This suggests that, as the system delocalizes, pairwise entanglement is the first type of entanglement to emerge—disappearing, however, in the chaotic region [25]. Such a disconnection between pairwise entanglement and the onset of chaos has also been verified for the 2D Ising model in a transverse field in [26] and, more recently, [27]. Contrary to that, each of the P_n decreases from nearly 1 to nearly 0, roughly corresponding to the transition in the LSI and ξ_c (cf. Fig. 1). Therefore, as we approach chaos, a shift from pairwise to genuinely multipartite entanglement occurs. Interestingly, in 1D a shift from short-range to long-range correlations is also noticeable, since a more pronounced decay is witnessed by P_1, which is subsequently followed by the other purities until finally being reached by P_6. In 2D, different P_n do not directly signify correlations over different distance, and all P_n curves superimpose more closely.

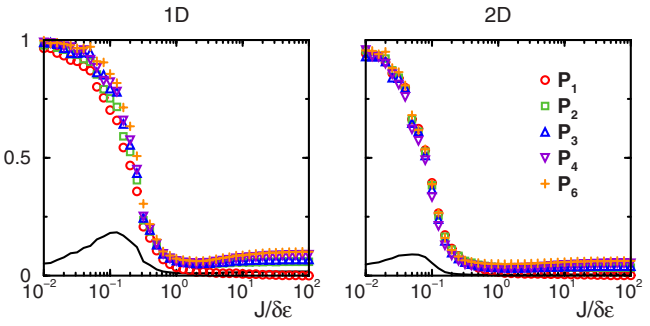

FIG. 6. (Color online) Case $J/\delta\varepsilon$. Average nearest-neighbor concurrence and n–local purity averaged over all eigenvectors of the $S_z=0$ subspace vs $\delta J/\delta\varepsilon$. Lattice size $L=12$. Solid black line: concurrence. Left panel: 1D chain. Right panel: 3×4 lattice. Averages over 20 random realizations.

In the region where $J/\delta\varepsilon$ increases from 1 to ∞ and the limiting Hamiltonian H_J is approached, C and P_1 are near zero throughout—note that, due to the rotational invariance of H_J, $P_1\to 0$ as $J/\delta\varepsilon\to\infty$, whereas P_2, P_3, P_4, and P_6 increase slightly, particularly in 1D. It is hard to ascertain whether this subtle variation in 1D is related to a transition to integrability or simply associated with the symmetry transition. Therefore, the similar entanglement behavior observed in both 1D and 2D does not mirror the differences in chaos between the two systems. In fact, it appears much more closely connected to the ξ_c behavior in this region. In this sense, a parallel between standard multipartite entanglement and delocalization is stronger than between the former and chaos. Furthermore, as in delocalization, the minimum values reached by each P_n in the central chaotic region, although low, do not attain the values predicted by RMT. For the 2D case, where agreement with RMT is best, the minimum of each P_n except for P_1 range between a factor of 4.5 and 5.8 times the RMT values in Table I. P_1 does attain the RMT value but only well into the S^2-symmetry region, where this effect cannot be attributed to chaos.

Case $\delta J/J$. Similar to the above case $J/\delta\varepsilon$ in the region $J/\delta\varepsilon\geq 1$, the entanglement behavior shows no qualitative difference between the 1D and 2D models for $\delta J/J\in[0,1]$, although an integrability-chaos transition occurs in 1D (see Fig. 7). On the other hand, both P_n and C change abruptly near $\delta J/J\sim 2$ in 1D, and near $\delta J/J\sim 3$ in 2D. In both cases, the sharp increase in pairwise entanglement and decrease in multipartite entanglement are paralleled by a decrease in ξ_c and, more interestingly, by an increase in the LSI (cf. Fig. 2). It is expected that the breaking of the chain into distinct subsystems will result in a decrease of multipartite entanglement. It is, however, intriguing that, although smaller, a decrease occurs also in 2D, where chain breaking should be suppressed.

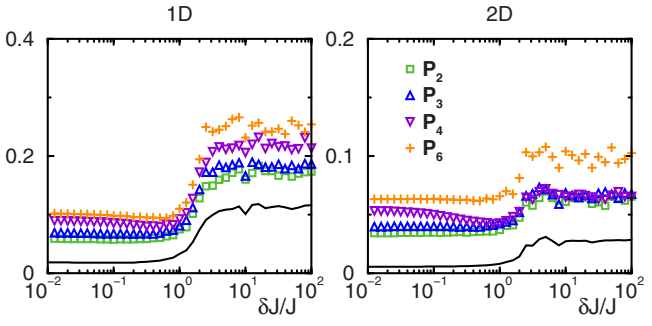

FIG. 7. (Color online) Case $\delta J/J$. Average nearest-neighbor concurrence and n–local purity averaged over all eigenvectors of the $(S_z,S)=(0,1)$ subspace vs $\delta J/J$. Lattice size $L=12$. Solid black line: concurrence. Left panel: 1D chain. Right panel: 3×4 lattice. Averages over 20 random realizations.

Case $\delta J/\delta\varepsilon$. The entanglement behavior in 2D for this disorder setting is very similar to the one depicted in the right panel of Fig. 6, whereas in 1D purities never reach low values, reflecting the lack of delocalization (cf. Fig. 3). We shall then focus on the 2D system and describe some interesting features of purity, which also apply to case $J/\delta\varepsilon$ in both 1D and 2D.

B. Energy and delocalization dependence

In addition to understanding how entanglement properties depend on disorder and interaction strength, their direct dependence upon energy and delocalization is relevant to gaining a more complete physical picture.

Similarly to the behavior observed for NPC within the TBRE (see Fig. 4), a strong correlation also exists between multipartite entanglement and the energy spectrum. The left panel of Fig. 8 contains a representative example for the bilocal purity. In general, states at the edges of the spectrum tend to be less entangled, whereas highly entangled states are clustered around intermediate energies. This result indicates a correspondence between P_n and the LDOS of the TBRE, which, as a function of energy, is Gaussian and broadly peaked at the center of the spectrum [67–69] (see also [23] for a discussion of the influence of LDOS properties on purity behavior). Essentially, where the LDOS is largest, a higher level of delocalization exists and also higher amounts

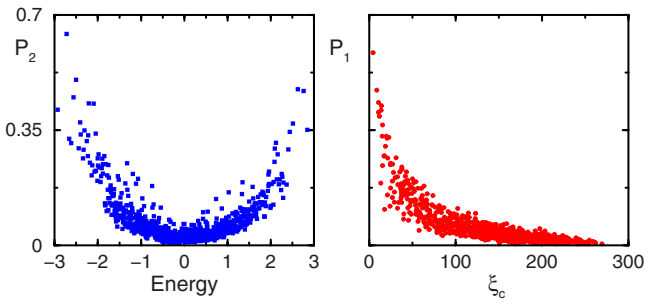

FIG. 8. (Color online) Case $\delta J/\delta\varepsilon$, $S_z=0$ subspace, 3×4 2D spin lattice, $\delta J/\delta\varepsilon=2$. Left panel: P_2 vs energy eigenvalue. Right panel: P_1 vs ξ_c. A single disorder realization is considered.

of multipartite entanglement occur. We emphasize, however, that this relationship is not *per se* indicative of chaos: A similar behavior was found for disordered on-site energies (case $J/\delta\varepsilon$) within the $(S_z,S,R)=(0,1,+1)$ sector for the 1D model in the limit $J/\delta\varepsilon\to\infty$, which corresponds to a delocalized, but integrable, regime.

The relationship between multipartite entanglement and delocalization may further be probed by directly comparing n-local purities and the NPC. A plot of the local purity P_1 as a function of delocalization in the c basis (right panel of Fig. 8) discloses a striking relationship between P_1 and ξ_c, which is found to persist for each of the P_n and for a broad range of values of $\delta J/\delta\varepsilon$ within the chaotic region (until the S^2 symmetry becomes strong). Remarkably, for a given P_n, the precise shape of the curve does *not* depend on $\delta J/\delta\varepsilon$, although it depends slightly on lattice dimension and disorder setting. The precise relationship between P_1 and ξ_c is examined at length in [93], where it is shown that the relationship between P_1 and ξ_c depends strongly on how correlated the state vector components are with respect to the *Hamming distance* between the quantum numbers describing c-basis states [94]. If no such Hamming correlation exists, inverse proportionality between local purity and NPC is expected (see also [23]):

$$P_1(|\psi\rangle)=\frac{N}{N-1}\frac{1}{\xi_c(|\psi\rangle)}-\frac{1}{N-1}\approx\frac{1}{\xi_c(|\psi\rangle)},$$

with $N=N_0=924$ for the central band. While this qualitatively agrees with the observed behavior, due to the fact that all interaction terms in the Hamiltonian are of a two-body nature, the components of the eigenvectors tend to be Hamming correlated, resulting in significant deviations from the predicted inverse scaling law, especially at small ξ_c. This effect was recently independently confirmed by Giraud and co-workers [95].

In addition to calling for a deeper understanding of the physical conditions leading to the observed nontrivial eigenvector structure, the above findings naturally prompt the following question: To what extent could the relationship between entanglement and delocalization provide a signature of quantum chaos? As a first step toward answering this question, we reconsider the case of a clean Heisenberg Hamiltonian H_J (case $J/\delta\varepsilon$ in the limit of no disorder), which supports both integrability (in 1D) and chaoticity (in 2D). Instead of P_1, which is identically zero for eigenvectors of $H=H_J$, we look at the block purity P_6. As illustrated in Fig. 9, no clear relationship between ξ_c and P_n emerges in the integrable regime (left panel), whereas a noticeable relationship is present in the chaotic case (right panel)—in spite of the limited statistics accessible due to symmetry constraints. Interestingly, this is in agreement with a recent study of entanglement and chaos for the Ising model in a transverse field by Lakshminarayan and co-workers [27], where a correlation between values of delocalization and block von Neumann entropy is found to occur only in chaotic regimes and not in integrable yet delocalized ones.

While the above results provide suggestive evidence in favor of using entanglement as a diagnostic tool for integrability, independent support is needed to rule out possible bias

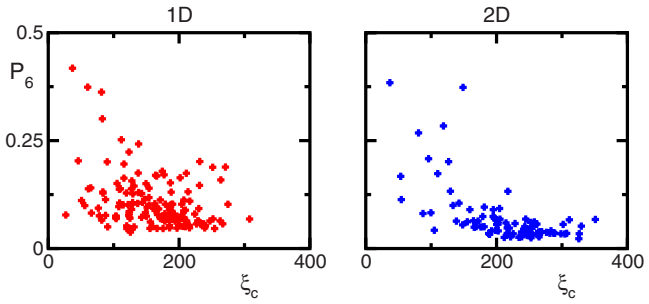

FIG. 9. (Color online) Multipartite entanglement vs delocalization in a clean Heisenberg Hamiltonian: P_6 vs ξ_c in the $(S_z,S,R)=(0,1,+1)$ symmetry subspace. Lattice size: $L=12$. Left panel: 1D chain. Right panel: 3×4 2D lattice.

due to the special relationship between multipartite entanglement and the c basis, or to the specific entanglement measure chosen. A natural option for circumventing such limitations is to invoke GE. In particular, the behavior of fermionic GE [as quantified by the $P_{u(L)}$-purity defined in Eq. (13)] as a function of delocalization in the c basis is depicted in Fig. 10 for the same clean 1D and 2D models examined above. Again, the observed delocalization dependence appears noticeably more pronounced in the 2D chaotic case, as opposed to the 1D integrable system. It is intriguing to think that this behavior ultimately reflects the fact that neighboring energy eigenstates possess common features in the chaotic regime, as argued by Zelevinsky and co-workers [50] (see also [96]). Although these findings reinforce the conjecture that, at least within the TBRE, a new entanglement-based signature of chaos may be identified in this way, validating this claim and its physical interpretation in more generality requires a dedicated investigation which we plan to present elsewhere.

VII. CONCLUSION AND OUTLOOK

We have provided a comprehensive quantitative analysis of spectral properties, delocalization, and entanglement for the eigenvectors of disordered spin-1/2 systems with Heisenberg interactions in one and two spatial dimensions. Disorder in the system has been introduced through random applied magnetic fields, random interactions, or both. Our main findings and conclusions may be summarized as follows.

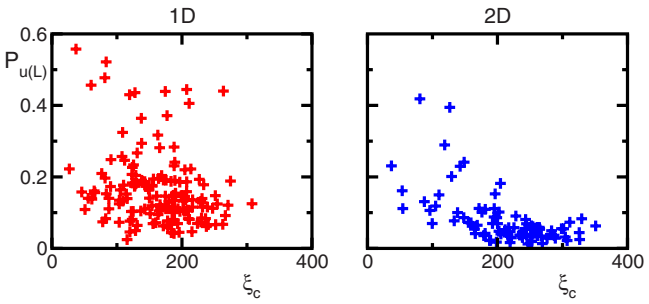

FIG. 10. (Color online) Generalized fermionic entanglement vs delocalization in a clean Heisenberg Hamiltonian: $P_{u(L)}$ vs ξ_c in the $(S_z,S,R)=(0,1,+1)$ subspace. Lattice size: $L=12$. Left panel: 1D chain. Right panel: 3×4 2D lattice.

(i) Although correspondence with nonintegrability is well documented, the interpretation of LSI data is, as expected, nontrivial in symmetry transition regions where invariant subspaces are partially overlapping—causing a tendency toward the Poisson distribution regardless of whether integrability is approached or not.

(ii) Standard NPC measures for state delocalization depend entirely on which basis is chosen to represent the eigenvectors of the Hamiltonian; thus they need not detect the transition from integrability to chaos if the latter is not accompanied by a significant change in the amount of delocalization. We have examined the effect of basis choice in two distinct bases of limiting integrable Hamiltonians as well as introduced a measure of relative, disorder-dependent delocalization which is shown to successfully detect quantum chaos in the presence of disorder. We find that delocalization, particularly in the computational basis, does not achieve the level predicted by RMT even in chaotic regions for the Heisenberg model. Low connectivity and the localizing nature of the Ising pairing are likely to play a role in accounting for such disagreement.

(iii) In delocalized systems, NPC and multipartite qubit entanglement show a dependence on energy that resembles the one observed for the density of states in the TBRE, reflecting a strong correlation among the three quantities. This complements findings on the influence of LDOS properties on dynamical aspects of entanglement in disordered qubit systems [23].

(iv) In the case where only random Heisenberg interactions are present, an interesting connection between level statistics, average eigenvector entanglement and delocalization, and the presence of a random singlet phase was uncovered in 1D. This may warrant further study, also in view of better elucidating what mutual relationships (if any) exist between quantum criticality and the ability of a system to sustain quantum chaos.

(v) Delocalization and multipartite entanglement both show a substantial increase during the transition from a localized integrable Hamiltonian to a chaotic one. Similar to NPC measures, both entanglement and GE measures are unavoidably relative to a choice of "local" resources—as captured by preferred subsystems or observables. However, comparison between two quantities sharing the same relative origin—NPC and P_n—results in a distinctive relationship which may serve as a quantum chaos indicator. Physically, such a relationship suggests that both entanglement and delocalization in a given local basis essentially capture the same information about eigenvector structure. Both the validity and implications of this potential entanglement signature, as well as a more substantial use of genuine GE, are points deserving additional in-depth investigation. In particular, a promising venue to explore is the possibility that GE measures relative to appropriate observable sets may allow to detect a transition to chaos starting from *any* integrable model, irrespective of its local or nonlocal nature with respect the the original operator language.

Finally, from a technical standpoint, the general method suggested in [93] and explicitly illustrated here for computing typical entanglement properties of random pure states

localized to a proper subspace of states in Hilbert space is likely to find broader applications within both quantum chaos and QIS.

ACKNOWLEDGMENTS

It is a pleasure to thank Viatcheslav V. Dobrovitski, Simone Montangero, and Yaakov S. Weinstein for valuable discussions and feedback. D.S.'s contribution to this work was initiated as part of an "Undergraduate Research Experience in Quantum Information Science" at SUNY Fredonia, NY. W.G.B. gratefully acknowledges partial support from the Constance and Walter Burke Special Projects Fund in Quantum Information Science, and from a GAANN grant.

APPENDIX: TYPICAL SUBSPACE ENTANGLEMENT: EXPECTED VALUES OF BLOCK PURITIES

Given the general expression of relative purity in Eq. (10), each P_n may be expressed as a sum of squared expectation values over a normalized, orthonormal, traceless basis $\{B_i\}$ for the distinguished observable set h. That is,

$$P_n(|\psi\rangle) = \kappa \sum_i \langle\psi|B_i|\psi\rangle^2,$$

where κ is a normalization factor ensuring that $\max_{|\psi\rangle}\{P_n\}=1$. Thus, the average purity over any ensemble of states is given by

$$\overline{P_n}(|\psi\rangle) = \kappa \sum_i \overline{\langle\psi|B_i|\psi\rangle^2}.$$

The method we shall follow to compute $\overline{P_n}$ will be based on the following result (proved in [93]).

Let $\mathcal{H}$ be a finite-dimensional Hilbert space, with dimension N, and let A be any traceless real symmetric operator on $\mathcal{H}$, normalized such that $\mathrm{tr}(A^2)=N$. Then for an ensemble of pure states $|\psi\rangle$ with real components taken uniformly with respect to the Haar measure on $O(N)$, the following relationship holds:

$$\overline{\langle\psi|A|\psi\rangle^2} = \frac{2}{N+2}.$$

For random states limited to a proper subspace, $\mathcal{S}\subset\mathcal{H}$, additional care must be taken because A need not be normalized or traceless after projection onto $\mathcal{S}$. Let $N'=\dim(\mathcal{S})$ and let Π denote the projector onto $\mathcal{S}$. If we let $\Pi A\Pi=\alpha A'+\beta\mathbb{1}$, where $\mathrm{tr}(A')=0$ and $\mathrm{tr}(A'^2)=N'$, it follows that

$$\overline{\langle\Pi A\Pi\rangle^2} = \frac{2\alpha^2}{N'+2} + \beta^2.$$

The coefficients α and β may be determined from $\mathrm{tr}(\Pi A\Pi)$ and $\mathrm{tr}[(\Pi A\Pi)^2]$,

$$\beta^2 = \frac{\mathrm{tr}(\Pi A\Pi)^2}{N'^2}, \quad \alpha^2 = \frac{\mathrm{tr}[(\Pi A\Pi)^2]}{N'} - \frac{\mathrm{tr}(\Pi A\Pi)^2}{N'^2},$$

respectively. Therefore, in order to calculate $\overline{P_n}$, the trace norm of both the projection $\Pi B_i\Pi$, and the projection squared, $(\Pi B_i\Pi)^2$, of each basis operator onto $\mathcal{S}$ must be determined.

Since in our case each P_n is an average over the purities of (L/n) n-qubit subsystems, it suffices to determine the average subsystem purity of a single n-qubit subsystem. A convenient operator basis is provided by the set of n-qubit Pauli operators, that is, all products of single-qubit Pauli operators and the identity, $B_i=\sigma_{\alpha_1}^{(1)}\otimes\cdots\otimes\sigma_{\alpha_n}^{(n)}$, where $\alpha_k=0$, x, y, or z. The choice of the identity σ_0 acting simultaneously on all qubits is excluded. It will be useful to consider the representation of the Pauli operators as matrices expressed in the standard c basis. The subspace $\mathcal{S}=\mathcal{H}_0$ of states with total $S_z=0$ angular momentum (no net magnetization) is relevant to our study, $N'=N_0$. The Pauli operators that have a nonvanishing projection into $\mathcal{H}_0$ are (1) those consisting of only σ_z and σ_0 operators; and (2) those consisting of an even number of σ_x and an even number of σ_y operators, with the remaining operators being any combination of σ_z and σ_0.

First, consider case 1. Each such operator is diagonal in the c basis, hence it remains diagonal after projection into $\mathcal{H}_0$. Because the eigenvalues of each such operator are ±1, $\mathrm{tr}(\Pi B_i\Pi)$ may be determined by simply counting the number of c basis states spanning $\mathcal{H}_0$ that correspond with each eigenvalue. For a Pauli string consisting of m σ_z and $(n-m)$ σ_0 operators, the number of c basis states with k 1's for the qubits acted on by the σ_z operators is $\binom{m}{k}\binom{L-m}{L/2-k}$. Thus,

$$\mathrm{tr}(\Pi B_i\Pi) = \sum_k (-1)^k \binom{m}{k}\binom{L-m}{L/2-k}.$$

If m is odd, then the above quantity is 0.

Next, consider case 2. Note that the effect of the operator $\sigma_x^{(i)}$ or $\sigma_y^{(i)}$ acting on a c-basis state is to flip the ith qubit from 0 to 1, or 1 to 0. Thus, for a c-basis state to remain in $\mathcal{H}_0$ after the action of a Pauli operator, the combined number of σ_x and σ_y operators must be even. Additionally, since every state in the ensemble has only real components in the c basis, those Pauli operators that have an odd number of σ_y have zero expectation value for each state in the ensemble. For a Pauli string with a total of m σ_x and σ_y operators, m 0's and 1's will be flipped when the operator acts on a c-basis state. Thus, the qubits acted on must have an equal number of 1's as 0's in order to remain in $\mathcal{H}_0$. There are $\binom{m}{m/2}$ possible assignments of 0's and 1's for such qubits. The remaining qubits (that is, those not acted upon by σ_x or σ_y operators) must also have an equal number of 1's as 0's since the state is in $\mathcal{H}_0$. There are $\binom{L-m}{(L-m)/2}$ possible assignments for such qubits. Therefore, there are $\binom{m}{m/2}\binom{L-m}{(L-m)/2}$ matrix elements in such a Pauli operator. Since each matrix element is 1, it follows that

$$\mathrm{tr}[(\Pi B_i\Pi)^2] = \binom{m}{m/2}\binom{L-m}{(L-m)/2}.$$

Since B_i acts nontrivially on every c-basis state, there are no diagonal elements and hence $\mathrm{tr}(\Pi B_i\Pi)=0$.

In order to properly normalize purity on an n-qubit subsystem, consider the pure c-basis state $|0,\ldots,0\rangle$. Only Pauli operators consisting of σ_z and σ_0 operators have nonvanish-

ing expectation values for this state, and each such expectation value is 1. There are (2^n-1) such operators; therefore $\kappa=1/(2^n-1)$ in this case.

With the above ingredients, $\overline{P_n}$ may be calculated by determining how many Pauli basis states for an n-qubit subsystem fall into each category described above in regard to trace norm and squared trace norm upon projection onto $\mathcal{H}_0$. We consider various coarse-grained purities separately.

(1) P_1. Only $\sigma_z^{(1)}$ has a nonvanishing expectation value. It has an odd number of σ_z operators; thus $\mathrm{tr}[(\Pi\sigma_z\Pi)^2]=N$ and $\mathrm{tr}(\Pi\sigma_z\Pi)=0$. Therefore,

$$\overline{P_1}=\frac{2}{N_0+2}.$$

(2) P_2. The Pauli operators with nonvanishing expectation values are $\sigma_z^{(1)}$, $\sigma_z^{(2)}$, $\sigma_z^{(1)}\sigma_z^{(2)}$, $\sigma_x^{(1)}\sigma_x^{(2)}$, and $\sigma_y^{(1)}\sigma_y^{(2)}$. Thus,

$$\overline{P_2}=\frac{1}{3}\left\{\frac{2}{N_0+2}\left[3-\frac{\lambda_2^2}{N_0^2}+\frac{4}{N_0}\binom{L-2}{(L-2)/2}\right]+\frac{\lambda_2^2}{N_0^2}\right\},$$

where for later purposes we let

$$\lambda_m=\sum_{k=0}^{k=m}(-1)^k\binom{m}{k}\binom{L-m}{L/2-k}.$$

(3) P_3. There are $\binom{n}{m}$ Pauli operators containing m σ_z and $(n-m)$ σ_0 operators, and in addition there are $2^{(n-2)}\binom{n}{2}$ Pauli operators containing two σ_x and $(n-2)$ σ_0 and σ_z operators and the same number of Pauli operators containing two σ_y and $(n-2)$ σ_0 and σ_z operators. This yields

$$\overline{P_3}=\frac{1}{7}\left\{\frac{2}{N_0+2}\left[7-\frac{3\lambda_2^2}{N_0^2}+\frac{24}{N_0}\binom{L-2}{(L-2)/2}\right]+\frac{3\lambda_2^2}{N_0^2}\right\}.$$

(4) P_4. All of the classes of Pauli operators listed for P_3 must be considered for P_4 also, with the following additional classes: the $2^{n-4}\binom{n}{2,2,n-4}$ Pauli operators with exactly two σ_x and two σ_y operators; the $2^{n-4}\binom{n}{4}$ Pauli operators with exactly four σ_x operators; and the $2^{n-4}\binom{n}{4}$ Pauli operators with exactly four σ_y operators. This yields

$$\overline{P_4}=\frac{1}{15}\left\{\frac{2}{N_0+2}\left[15-\frac{6\lambda_2^2}{N_0^2}-\frac{\lambda_4^2}{N_0^2}+\frac{48}{N_0}\binom{L-2}{(L-2)/2}+\frac{8}{N_0}\binom{L-4}{(L-4)/2}\right]+\frac{6\lambda_2^2}{N_0^2}+\frac{\lambda_4^2}{N_0^2}\right\}.$$

(5) P_6. The additional classes of Pauli operators to contribute to P_6 are the $2^{n-6}\binom{n}{4,2,n-6}$ Pauli operators with exactly four σ_x and two σ_y operators; the $2^{n-6}\binom{n}{2,4,n-6}$ Pauli operators with exactly two σ_x and four σ_y operators; the $2^{n-6}\binom{n}{6}$ Pauli operators with exactly six σ_x operators; and the $2^{n-6}\binom{n}{6}$ Pauli operators with exactly six σ_y operators. This yields

$$\overline{P_6}=\frac{1}{63}\left\{\frac{2}{N_0+2}\left[63-\frac{15\lambda_2^2}{N_0^2}-\frac{15\lambda_4^2}{N_0^2}-\frac{\lambda_6^2}{N_0^2}+\frac{480}{N_0}\binom{L-2}{(L-2)/2}+\frac{480}{N_0}\binom{L-4}{(L-4)/2}+\frac{32}{N_0}\binom{L-6}{(L-6)/2}\right]+\frac{15\lambda_2^2}{N_0^2}+\frac{15\lambda_4^2}{N_0^2}+\frac{\lambda_6^2}{N_0^2}\right\}.$$

Letting $L=12$, $N_0=924$ in the above formulas leads to the n–local purity values quoted in Table I.

[1] E. P. Wigner, Ann. Math. **62**, 548 (1955); E. P. Wigner, *ibid.* **65**, 203 (1957); E. P. Wigner, *ibid.* **67**, 325 (1958).

[2] F. M. Izrailev, Phys. Rep. **196**, 299 (1990).

[3] M. L. Mehta, *Random Matrices* (Academic Press, Boston, 1991).

[4] T. Guhr, A. Mueller-Gröeling, and H. A. Weidenmüller, Phys. Rep. **299**, 189 (1998).

[5] M. A. Nielsen and I. L. Chuang, *Quantum Computation and Quantum Information* (Cambridge University Press, Cambridge, U.K., 2000).

[6] G. Benenti, G. Casati, and G. Strini, *Principles of Quantum Computation and Information: Basic Tools and Special Topics* (World Scientific, Singapore, 2007).

[7] B. Georgeot and D. L. Shepelyansky, Phys. Rev. E **62**, 6366 (2000).

[8] B. Georgeot and D. L. Shepelyansky, Phys. Rev. E **62**, 3504 (2000).

[9] A. Harrow, P. Hayden, and D. Leung, Phys. Rev. Lett. **92**, 187901 (2004); C. H. Bennett, P. Hayden, D. Leung, P. Shor, and A. Winter, IEEE Trans. Inf. Theory **51**, 56 (2005).

[10] E. Schrödinger, Naturwiss. **23**, 807 (1935).

[11] L. Amico, R. Fazio, A. Osterloh, and V. Vedral, Rev. Mod. Phys., arXiv:quant-ph/0703044.

[12] F. D. Verstraete, D. Porras, and J. I. Cirac, Phys. Rev. Lett. **93**, 227205 (2004); G. Vidal, *ibid.* **91**, 147902 (2003); **93**, 040502 (2004).

[13] P. A. Miller and S. Sarkar, Phys. Rev. E **60**, 1542 (1999).

[14] M. Znidaric and T. Prosen, J. Phys. A **36**, 2463 (2003).

[15] A. J. Scott and C. M. Caves, J. Phys. A **36**, 9553 (2003).

[16] P. Jacquod, Phys. Rev. Lett. **92**, 150403 (2004).

[17] S. Ghose and B. C. Sanders, Phys. Rev. A **70**, 062315 (2004).

[18] X. Wang, H. Li, and B. Hu, Phys. Rev. A **69**, 054303 (2004).

[19] J. N. Bandyopadhyay and A. Lakshminarayan, Phys. Rev. Lett. **89**, 060402 (2002).

[20] J. N. Bandyopadhyay and A. Lakshminarayan, Phys. Rev. E **69**, 016201 (2004).

[21] A. Lakshminarayan and V. Subrahmanyam, Phys. Rev. A **71**, 062334 (2005).

[22] Y. S. Weinstein and C. S. Hellberg, Phys. Rev. Lett. **95**, 030501 (2005).

[23] S. Montangero and L. Viola, Phys. Rev. A **73**, 040302(R) (2006).

[24] A. Lakshminarayan and V. Subrahmanyam, Phys. Rev. A **67**,

052304 (2003).
[25] L. F. Santos, G. Rigolin, and C. O. Escobar, Phys. Rev. A **69**, 042304 (2004).
[26] C. Mejia-Monasterio, G. Benenti, G. G. Carlo, and G. Casati, Phys. Rev. A **71**, 062324 (2005).
[27] J. Karthik, A. Sharma, and A. Lakshminarayan, Phys. Rev. A **75**, 022304 (2007).
[28] D. Loss and D. P. DiVincenzo, Phys. Rev. A **57**, 120 (1998).
[29] D. P. DiVincenzo, D. Bacon, J. Kempe, G. Burkard, and K. B. Whaley, Nature (London) **408**, 339 (2000).
[30] B. E. Kane, Nature (London) **393**, 133 (1998).
[31] M. I. Dykman and P. M. Platzman, Fortschr. Phys. **48**, 1095 (2000).
[32] D. Bacon, K. R. Brown, and K. B. Whaley, Phys. Rev. Lett. **87**, 247902 (2001).
[33] M. I. Dykman and L. F. Santos, J. Phys. A **36**, L561 (2003).
[34] L. F. Santos and M. I. Dykman, Phys. Rev. B **68**, 214410 (2003).
[35] Y. S. Weinstein, C. S. Hellberg, and J. Levy, Phys. Rev. A **72**, 020304(R) (2005).
[36] H. Barnum, E. Knill, G. Ortiz, and L. Viola, Phys. Rev. A **68**, 032308 (2003).
[37] H. Barnum, E. Knill, G. Ortiz, R. Somma, and L. Viola, Phys. Rev. Lett. **92**, 107902 (2004).
[38] R. Somma, G. Ortiz, H. Barnum, E. Knill, and L. Viola, Phys. Rev. A **70**, 042311 (2004).
[39] Y. S. Weinstein and L. Viola, Europhys. Lett. **76**, 746 (2006).
[40] R. Somma, H. Barnum, G. Ortiz, and E. Knill, Phys. Rev. Lett. **97**, 190501 (2006).
[41] F. Haake, *Quantum Signatures of Chaos* (Springer-Verlag, Berlin, 1991).
[42] V. V. Flambaum and F. M. Izrailev, Phys. Rev. E **56**, 5144 (1997).
[43] V. V. Flambaum, A. A. Gribakina, G. F. Gribakin, and I. V. Ponomarev, Physica D **131**, 205 (1999).
[44] S. Weigert, Physica D **56**, 107 (1992).
[45] A. Enciso and D. Peralta-Salas, Theor. Math. Phys. **148**, 1086 (2006).
[46] V. V. Flambaum, Aust. J. Phys. **53**, 489 (2000).
[47] E. K. Sklyanin, in *Quantum Groups and Quantum Integrable Systems*,edited by Mo-Lin Ge, Nankai Lectures in Mathematics and Physics (World Scientific, Singapore, 1992).
[48] P. Jacquod and I. Varga, Phys. Rev. Lett. **89**, 134101 (2002).
[49] P. Jacquod and D. L. Shepelyansky, Phys. Rev. Lett. **79**, 1837 (1997).
[50] V. Zelevinsky, B. A. Brown, N. Frazier, and M. Horoi, Phys. Rep. **276**, 85 (1996).
[51] Different conventions and terminology are found in the literature. In fact, there are at least three names given to the quantity defined in Eq. (5): In addition to the NPC terminology we follow here [see, e.g., V. K. B. Kota and R. Sahu, Phys. Rev. E **64**, 016219 (2001)], the NPC is also referred to as the *participation number* (PN) in [26]. Furthermore, the definitions of NPC vs IPR are often interchanged, as in [23]. Adding to the confusion, there is overlap in terminology with a similar measure of *mixedness*, $[\mathrm{tr}(\rho^2)]^{-1}$, which is also, sometimes, referred to as either IPR or PN.
[52] G. P. Berman, F. Borgonovi, F. M. Izrailev, and V. I. Tsifrinovich, Phys. Rev. E **64**, 056226 (2001).
[53] E. Chudnovsky and J. Tejada, *Lectures on Magnetism* (Rinton Press, Paramus, NJ, 2006).
[54] T. C. Hsu and J. C. Angles d'Auriac, Phys. Rev. B **47**, 14291 (1993).
[55] K. Kudo and T. Deguchi, J. Phys. Soc. Jpn. **74**, 1992 (2005).
[56] D. A. Rabson, B. N. Narozhny, and A. J. Millis, Phys. Rev. B **69**, 054403 (2004).
[57] Y. Avishai, J. Richert, and R. Berkovits, Phys. Rev. B **66**, 052416 (2002).
[58] L. F. Santos, J. Phys. A **37**, 4723 (2004).
[59] K. Kudo and T. Deguchi, Phys. Rev. B **69**, 132404 (2004).
[60] R. Vrijen, E. Yablonovitch, K. Wang, H. W. Jiang, A. Balandin, V. Roychowdhury, T. Mor, and D. P. DiVincenzo, Phys. Rev. A **62**, 012306 (2000).
[61] L.-A. Wu and D. A. Lidar, Phys. Rev. A **67**, 050303(R) (2003).
[62] Y. S. Weinstein and C. S. Hellberg, Phys. Rev. Lett. **98**, 110501 (2007).
[63] L. Viola, E. Knill, and S. Lloyd, Phys. Rev. Lett. **82**, 2417 (1999); L. Viola and E. Knill, *ibid.* **90**, 037901 (2003); **94**, 060502 (2005).
[64] We verified that using Gaussian-distributed random numbers in place of uniform random numbers produced no significant qualitative difference.
[65] J. B. French and S. S. M. Wong, Phys. Lett. **33B**, 449 (1970).
[66] O. Bohigas and J. Flores, Phys. Lett. **34B**, 261 (1971).
[67] T. A. Brody, J. Flores, J. B. French, P. A. Mello, A. Pandey, and S. S. M. Wong, Rev. Mod. Phys. **53**, 385 (1981).
[68] V. K. B. Kota and R. Sahu, Phys. Lett. B **429**, 1 (1998).
[69] V. K. B. Kota, Phys. Rep. **347**, 223 (2001).
[70] Technically, for the TBRE, recovery of GOE statistics requires unfolding the spectrum of each member individually, as implemented in our numerical procedure.
[71] A set of mutually commuting operators acting on Hilbert space $\mathcal{H}$ is *complete* if and only if their corresponding eigenvalues label a basis of $\mathcal{H}$.
[72] As a particular feature of the $S_z=0$-subspace of $\mathcal{H}_0$, note that it is also invariant under the discrete transformation $Z_2=\otimes_{i=1}^{L}\sigma_x^{(i)}$, which is associated with a global π rotation about the x axis. However, since the value of the total angular momentum determines the irreducible representation according to which each state transforms under rotations, such a Z_2 symmetry is not independent of S^2, and consequently does not induce additional invariant subspaces.
[73] T. Guhr and H. A. Weidenmüller, Ann. Phys. (N.Y.) **199**, 412 (1990).
[74] A. A. El-Hady, A. Y. Abul-Magd, and M. H. Simbel, J. Phys. A **35**, 2361 (2002).
[75] L. F. Santos, Phys. Rev. A **67**, 062306 (2003).
[76] M. I. Dykman, L. F. Santos, and M. Shapiro, J. Opt. B: Quantum Semiclassical Opt. **7**, S363 (2005).
[77] H. A. Bethe, Z. Phys. **71**, 205 (1931).
[78] C. N. Yang and C. P. Yang, Phys. Rev. **150**, 321 (1966).
[79] F. C. Alcaraz, M. N. Barber, and M. T. Batchelor, Ann. Phys. (N.Y.) **182**, 280 (1988).
[80] M. Karbach and G. Müller, Comput. Phys. **11**, 36 (1997).
[81] V. V. Sokolov, B. A. Brown, and V. Zelevinsky, Phys. Rev. E **58**, 56 (1998).
[82] Both reflection subspaces with $S=1$ possess approximately Poisson distribution at $\delta\varepsilon=0$. This was verified on a 14-qubit chain to get better statistics. An analysis of the overall distri-

bution across all symmetry subspaces of a seven-qubit chain was carried out in [54].
[83] S. K. Ma, C. Dasgupta, and C. K. Hu, Phys. Rev. Lett. **43**, 1434 (1979).
[84] C. Dasgupta and S. K. Ma, Phys. Rev. B **22**, 1305 (1980).
[85] R. N. Bhatt and P. A. Lee, Phys. Rev. Lett. **48**, 344 (1982).
[86] Note that the transition to nonintegrability occurs at a larger value than in the other disorder settings, e.g., $\delta J/\delta\varepsilon \sim 10$ in 1D. The reason for this shift is simply the fact that, given the parametrization used, the range of the interaction is chosen, but the ratio between the *average* interaction strength and the on-site disorder strength should be considered for a fair comparison.
[87] W. K. Wootters, Phys. Rev. Lett. **80**, 2245 (1998).
[88] D. M. Greenberger, M. Horne, and A. Zeilinger, *Bell's Theorem, Quantum Theory, and Conceptions of the Universe* (Kluwer, Dordrecht, 1989).
[89] A. J. Scott and C. Caves, J. Phys. A **36**, 9553 (2003).
[90] L. Viola and H. Barnum, *Philosophy of Quantum Information and Entanglement*, edited by Alisa Bokulich and Gregg Jaeger (Cambridge University Press, Cambridge) (in press).
[91] D. Meyer and N. Wallach, J. Math. Phys. **43**, 4273 (2002).
[92] G. Brennen, Quantum Inf. Comput. **3**, 619 (2003).
[93] L. Viola and W. G. Brown, J. Phys. A **40**, 8109 (2007).
[94] Given two binary strings of equal length, the Hamming distance counts the number of substitutions needed to change one into the other. Physically, this has a simple interpretation in terms of spin-flip operations.
[95] O. Giraud, J. Martin, and B. Georgeot, Phys. Rev. A **76**, 042333 (2007).
[96] I. Percival, J. Phys. B **6**, L229 (1973).